Title

Damage assessment with state–space embedding strategy and singular value decomposition under stochastic excitation

Journal

Structural Health Monitoring, 13(2)

ISSN

1475-9217

Authors

Liu, Gang
Mao, Zhu
Todd, Michael
et al.

Publication Date

2014-03-01

DOI

10.1177/1475921713513973

Peer reviewed

Damage Assessment with State-Space Embedding Strategy and Singular Value Decomposition under Stochastic Excitation

Gang Liu[1,2], Zhu Mao[3], Michael Todd,[3] and Zongming Huang[1,2]

Abstract A multivariate time series analysis employing a state-space embedding strategy and singular value decomposition is presented in this article to detect infrastructure damage. After summarizing the current state space reconstruction method, the univariate state-space reconstruction is extended to multivariate (or global) reconstruction for observed time series at multiple locations. Under the hypothesis that reconstructed phase state geometry will change with damage, a reduced feature based on Mahalanobis distance (MD) of the most significant singular value vector, which is calculated from the reconstructed trajectory, is proposed. Both the area under receiver operating characteristic (ROC) curve and deflection coefficient (DC) are used as comparison metrics to illustrate the presence and severity of damage. The advantage of this proposed approach is computational efficiency and easy implementation using state-space methodology, since it does not require high-dimensional neighbor searches, as previous methods have proposed. Validation of the approach is demonstrated using a 6-degree-of-freedom linear spring mass system and the IASC-ASCE 4-story benchmark experimental structure. Results from both test-beds show that damage occurrence and severity can be successfully identified.

Keywords: structural health monitoring, damage detection, singular value decomposition, state-space reconstruction, receiver operating characteristics, deflection coefficient

1 Introduction

Aging civil infrastructure inevitably deteriorates under operational loading and environmental conditions, and structural failure may result in serious economic, performance, or life-safety consequences. The field of structural health monitoring (SHM) has evolved rapidly in civil infrastructure assessment, especially using damage methodologies relying on in-service measurement of performance such as vibration. This category of SHM strategies extracts damage-sensitive features from the dynamic response of structures, under the assumption that damage will change the fundamental structural characteristics observed in the vibration, such as mass, stiffness, damping,

[1]School of Civil Engineering, Chongqing University, Chongqing, 400045, China

[2]Key Laboratory of New Technology for Construction of Cities in Mountain Area (Chongqing University), Ministry of Education, Chongqing, 400045, China

[3]Department of Structural Engineering, University of California, San Diego, La Jolla, CA, 92093-0085, U.S.A

connectivity, etc. A large range of literature about this methodology is reviewed by Doebling et al. [1], Sohn et al. [2], and Farrar et al. [3].

A major subset of this methodology concerns model-based or model-enhanced procedures, including (but not limited to) modal frequency variations, modal shape-related indices [2], dynamical flexibility [3] and FEM model updating [4]. These dynamic models describe global structural characteristics explicitly, but they often fail at identifying systems with damage-induced nonlinearities and typically require heavy computational/processing loads (especially model updating). Some of these problems are reviewed by a comparative study in [5]. Beyond model-based methods, statistical time series analysis (data-driven method) comprise another large set of approaches in SHM, which extracts damage sensitive features directly from measured data ("data mining"), so that the complexity of global system identification is avoided and online damage diagnosis can be more easily implemented. Data-based methods have been intensively investigated, and many damage detection approaches have been developed based on, for example, autoregressive (AR) models [6], auto-regressive moving average (ARMA) models [7], auto-regressive model with exogenous input (ARX) [8,9], wavelets [10], and the Hilbert-Huang transform [11].

A novel suite of damage diagnostic methodologies based on the geometric variation of a system's dynamic state space has been proposed and implemented by Todd, Nichols, Trendafoilova, Moniz, Fasel, Torkamani et al. [12-18] in recent years. It is known according to the theories of embedology that a dynamic system may be described by its reconstructed (from data) state space. Topology changes in the state space, therefore, can be regarded as a new category of features that may distinguish different conditions of the structure before and after damage. The most widely used features utilizing geometry of state space include average local attractor variance ratio [12], auto-prediction error [13], cross-prediction error [14], chaotic amplification of attractor distortion, and correlation dimension of attractors [15]. Previous studies have demonstrated that this method can improve an order-of-magnitude in resolution and robustness over several traditional modal-based features [12]. Furthermore, due to independence on underlying physics, nonlinearity-induced damage, such as opening and closing of cracks, can be successfully detected by such approaches.

In order to improve sensitivity and avoid the influence of noise, all the above-mentioned state-space-based studies use well-tailored chaotic excitations; however, this is often impractical or expensive in civil infrastructure applications to apply deterministic and/or user-defined input to the system. Nichols et al. tried stochastic excitation conforming to the Pierson-Moskowitz wave distribution to detect and quantify damage of offshore structures [19]. Overbey et al. explored band-limited stochastic excitation to discern bolt loosening in a single-bay steel frame [20]. Nie et al. successively detected and localized damage on a circular steel arch test bed under impact excitation [21]. These three applications have conceptually demonstrated that the state-space based methodology without applied chaotic excitation can also be used to diagnose damage, but it has been only implemented on relative simple structures and insufficiently explored for SHM on more realistic systems. One of the objectives of this article is to present a state-space based feature extraction application under stochastic excitation and to apply the proposed

feature to diagnose damage in more complicated structures. In this work, the fundamental hypothesis is that singular value spectrum of the reconstructed trajectory reveals the damage-induced geometric changes to the system, and Mahalanobis distance (MD) of the singular value vector from baseline to test case is used as a metric ("feature") to quantify the changes. Two statistical evaluations, namely receiver operating characteristics and the deflection coefficient, are then used to determine significance of the change and are further interpreted for higher-level evaluation, such as severity.

The paper is organized as follows: Section 2 gives a brief overview of state space reconstruction along with parameter selection methods. Section 3 describes the proposed approach and its procedure for damage diagnosis. Section 4 provides a description of a simulated 6 degree-of-freedom system and then a realistic test structure (the ASCE benchmark test structure). Section 5 and section 6 present discussion of the test results and summarize the analysis workflow, respectively.

2 State-space embedding strategy and parameter selection method

2.1 Global attractor reconstructions

Time evolution of multi-degree-of-freedom linear dynamical systems can be typically described by the second order differential equation:

$$[M]\{\ddot{u}(t)\}+[C]\{\dot{u}(t)\}+[K]\{u(t)\}=\{F\} \tag{1}$$

where $[M]$, $[C]$, and $[K]$ are the mass, damping, and stiffness matrices of the system, respectively, $\{u(t)\}$ is the displacement vector, and $\{F\}$ is the input force vector. From the state model point of view, this differential equation can be transformed to a state-space representation:

$$\begin{cases} \{\dot{x}(t)\}=\underbrace{\begin{bmatrix} [0] & [I] \\ -[M]^{-1}[K] & -[M]^{-1}[C] \end{bmatrix}}_{A}\{x(t)\}+\begin{bmatrix} [0] \\ [M]^{-1} \end{bmatrix}\{F\} \\ \{y\}=\begin{bmatrix} [I] & [0] \end{bmatrix}\{x(t)\} \end{cases} \tag{2}$$

where $\{x\}$ is the state vector variable, including displacement and velocity of all degrees of freedom and $\{y\}$ is the observed output. Using each variable as a coordinate variable, the observed output of Equation (2) will trace out a trajectory in state space when the input force is deterministic, and the trajectory will approach the system's dynamic attractor under a steady-state condition. When damage occurs, the matrix $\boldsymbol{A}$ is expected to change, the attractor will vary correspondingly. Therefore, the "geometry" change of the attractor will reflect the damage-induced changes of the system [19].

In practice, of course, it is very difficult to measure each of the system's state variables directly, and usually only scalar data are available from a sensor network. However, the state space may be reconstructed via the embedding theorem of Takens using a delay coordinate approach if the reconstruction dimension $m \geq 2z+1$, where z is the box-counting dimension of the dynamic system [22]. The m-dimensional attractor at time i can be expressed as,

$$\{B_i\} = \{y_i, y_{i+\tau}, ..., y_{(i+m-1)\tau}\} \quad (3)$$

where τ is a time delay and y is the measured scalar signal. Mathematically, this procedure converts the scalar measured series y into a series of vectors $\{B\}$. Under stochastic excitation, there is no attractor in theory since the state-space geometry (attractor) will be infinite dimensional, but band-limited stochastic excitation can be evaluated as low-dimensional deterministic processes. With theoretical foundations of stochastic embedding established recently, several works have applied the reconstructed attractor under stochastic excitation to identify damages [20].

When data from l sensor channels can be obtained, equation (3) describing the univariate case can be extended to multivariate case for state-space reconstruction [23] in the form of:

$$\{B_i\} = \{y_i^1, y_{i+\tau_1}^1, ..., y_{i+(m_1-1)\tau_1}^1, y_i^2, ..., y_{i+(m_2-1)\tau_2}^2, ..., y_i^l, ...y_{i+(m_l-1)\tau_l}^l\} \quad (4)$$

where τ_i and m_i are time delay and embedding dimension for the i-th sensor channel. The global attractor is acquired by combining structural response data measured at multiple locations through the above equation and then the global embedding dimension is $M=m_1 + m_2 +\ldots+ m_l$.

2.2 Optimal embedding parameter selection methods

From equation (3) and (4), a successful attractor reconstruction requires optimal choice of embedding parameters, including time delay τ and embedding dimension m for each sensor channel. There are several proposed methods for optimizing parameter selection, and only those universally-used methods will be considered in this paper.

A proper time delay is chosen to make vector coordinates (columns of the reconstructed attractor) linearly uncorrelated; two quantities—autocorrelation function and average mutual information (AMI)—are often used to find that optimal time delay. As autocorrelation function cannot capture nonlinear relationships among time series, the AMI method is adopted in this paper. AMI measures the general dependence of two variables by the AMI function [24] and the time scale T corresponding to the first local minimum of this function is used as the optimal time delay.

A proper embedding dimension will geometrically capture the dynamics of a system adequately without redundant coordinates. The most commonly used approach is the false nearest neighbor (FNN) method [25, 26]. In this FNN algorithm, the false neighbor is defined as two neighboring points in the i^{th} dimension of state space, but geometrically far away in the $(i+1)^{th}$ dimension. In other words, with an increasing number of projected dimensions, the false neighbors will no longer be actual neighbors. Therefore, when the adequate minimum unfolding dimension m is reached, the percentage of false nearest neighbor projections should decline to zero, and thus the appropriate embedding is determined.

3 The proposed damage detection method

3.1 Singular value decomposition

As mentioned, the fundamental hypothesis is that the attractor will change after damage. Traditionally, internal variation of the attractor is used as metric to quantify this change, such as auto-prediction error and cross-prediction error obtained from a variety of mappings between reference and test attractors [20]. These mappings primarily consider central tendencies (low-order statistical properties) of the error as indicative of damage, but it is investigated in this paper whether some kinds of damage induces more "extreme value" behavior in the trajectories, which would be reflected more in changes in the boundary of the attractor, whose properties are shown to be related to the resulting singular value spectrum when the attractor is mapped through its singular vector matrix.

To remove the first order homogeneous attractor size changes simply due to global signal-to-noise change or excitation amplitude fluctuation, the measured data are normalized to zero mean and unit standard deviation before attractor reconstruction. In order to capture the periphery variations of the reconstructed attractor before and after damage without heavy computation, singular values of the reconstructed attractor are extracted by singular value decomposition technique [27]:

$$M = U\Sigma V^{*} \tag{5}$$

where M is reconstructed attractor and U and V are unitary matrix respectively and $\Sigma$is a diagonal matrix with all singular values (nonnegative real numbers $\sigma_i, \sigma_1 > \sigma_2 > .. > \sigma_n$) on the diagonal. A heuristic understanding of the proposed damage detection methodology is presented in Fig 1 using two-dimension attractor example.

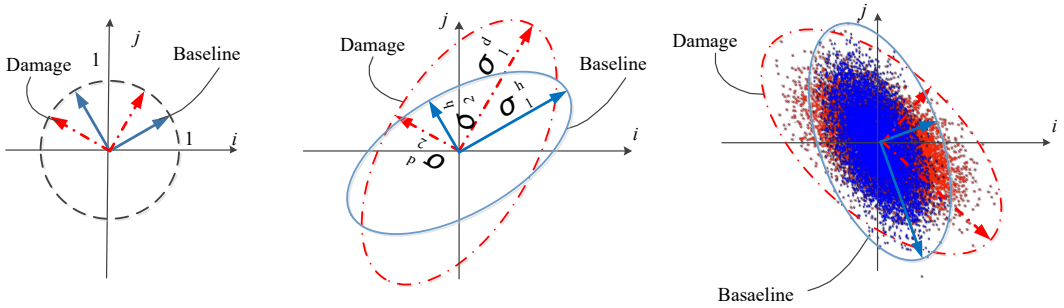

(a) (b) (c)

Figure 1: Geometry interpretation for the proposed method (a) unit circle (b) scaling (c) rotation

Since V is unitary matrix, each column vector of V describe points on unit circle for a 2D case, which is plotted in Fig. 1(a) with red dashed arrows as damaged condition and blue arrows as baseline condition respectively. Fig. 1(b) describes operation $E = \Sigma V^{*}$, which can be viewed as scaling the unit circle to ellipse according to each of the singular values

(diagonal entries of matrix Σ). The first singular value (σ_1^d and σ_1^h in Fig. 1(b), superscript *d* and *h* describe damage and baseline respectively) is the long semi-axis of the ellipse. Fig. 1(c) describes operation $M = UE$, which can be interpreted as procedure of acquiring the original attractor by rotation. In *n*-dimension case, the attractor can be thought as exploring on average an *n*-dimension ellipsoid, and σ_i is the length of the *i*-th semi-axis of this ellipsoid. Therefore, singular values are essentially of the dimension of periphery of the attractor and can be utilized as metric to identified damage. Moreover, advantage of the proposed method is that the algorithm can be executed rapidly and efficiently, since internal trajectory information, such as the variation of trajectory neighbor points (which can require nearest-neighbor searching in a high-dimensional space), is not required, as it was for many of the previous methods referenced above.

3.2 Damage features and the damage detection procedure

After the singular values are acquired (resulting in a vector of such values), the Mahalanobis distance (MD) is used as dissimilarity measure from the reference condition and is proposed as the fundamental damage detection scalar metric. MD is simply the distance of the test point from the center of mass divided by the width of the ellipsoid in the direction of the test point. The definition of MD is [28]

$$MD(\sigma) = \sqrt{(\sigma - \bar{\sigma})^T W^{-1} (\sigma - \bar{\sigma})} \tag{6}$$

where σ is a multivariate vector $\sigma = \{\sigma_1, \sigma_2, ..., \sigma_n\}^T$ in which σ_i describes the *i*-th singular value; $\bar{\sigma}$ and *W* are respectively the mean and covariance of a matrix, which is composed of singular values when the structure is under the baseline condition.

In order to measure detection performance of the proposed method, the area under a receiver operating characteristic (ROC) curve (AUC) is adopted in this study, which is a statistical metric indicating the detection performance of the feature (correct detections or classifications vs. false positives) as function of decision threshold. The metric ranges from 1, which perfect detection or classification independent of threshold, to 0.5, which represents a detection or classification performance equivalent to a random guess. More detailed discussions about the theory of AUCs and ROCs can be found in [30].

In addition to using AUC for performance comparison, deflection coefficient (DC) is used to evaluate damage severity, which is defined by

$$DC = \frac{\kappa_d - \kappa_h}{\sigma_h^2 + \sigma_d^2} \tag{7}$$

where subscription *d* and *h* represent damage and baseline condition respectively, κ and σ is the average and standard deviation of the MD. In the current formulation of using the MD of the singular value spectrum as the feature, increasing damage is expected to cause a corresponding mean shift in the MD without significant change in variance (without increasing feature evaluation uncertainty), implying that the DC might be useful as a severity measure.

The damage-detection algorithm is summarized in the following steps:

1). Populate two databases X_h and X_d from the health and damaged structure respectively.

2). Divide each database into a series of segments $S_{h,i}$ and $S_{d,i}$ (i=1,2,…,n) while the length of each segment is the same, and then regularize each segment to remove all first-order trends from nonstationarity, such as trend due to environmental conditions.

3). Reconstruct attractor $A_{h,i}$ and $A_{d,i}$ from $S_{h,i}$ and $S_{d,i}$ using proper time delay and dimension respectively given by Equation (4).

4). Compute the singular value vector $\sigma_{h,i}$ for each $A_{h,i}$ by singular value decomposition technique, and if singular values are zero, they will be discarded. Cluster half of these vectors to form a baseline subset $\sigma_{b,k}$ and the others to form reference subset $\sigma_{r,k}$ respectively (k=1,2,…,n/2).

5). Calculate the mean and variance of singular value using all baseline subset $\sigma_{b,k}$.

6). Obtain logarithmic Mahalanobis distance $DM_{h,k}$ as reference by Equation (6) using the reference subset $\sigma_{r,k}$.

7). Compute the singular value vector $\sigma_{d,i}$ just using half number of $A_{d,i}$, and calculate logarithmic $DM_{d,k}$ (k=1, 2,…,n/2) by equation (6) as testing.

8). Use AUC as statistical metric to quantify the performance of damage detection.

9). Evaluate damage severity with the DC.

This procedure of this method executes an eigen-analysis of the embedding matrix, in which each dimension (column) is a delayed version of the time series obtained from each sensor, and the procedure is similar to the process of finding the periphery of an ellipsoid (attractor). Moreover, the logical system of the state-space based method is rigorous, so the proposed method is discussed in the framework of the attractor.

4 Test description

4.1 Computational model

Before experimental evaluation, a relatively simple 6-DOF spring-mass system is designed to test the proposed method, which is shown in Fig.2. Initial spring stiffness is k_i=1500 (i=1…6) and mass values is m_i=1 (i=1,…,6). The damping matrix C is set as Rayleigh damping, C=0.01*K +0.00015 *M, which is a linear combination of stiffness matrix K and mass matrix M.

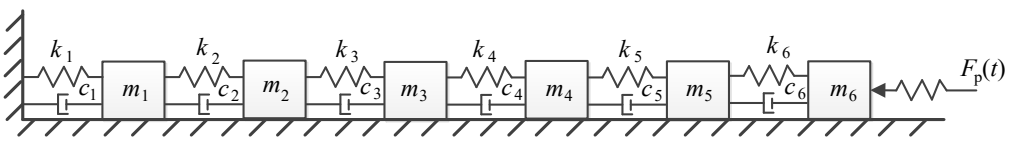

Figure 2: 6 degree-of-freedom mass and spring system

Stochastic excitation is applied at the right end of the structure, and the acceleration responses from m_1 to m_6 are recorded as multivariable output. Damage is simply

simulated as loss of spring stiffness. Different damage scenarios and the corresponding natural frequencies of undamped system are listed in Table 1.Note that the natural frequencies do not change drastically until severe damage occurs in the system, such as cases 3 and 4.

Table 1: Damage case and corresponding frequency

case	k	w_1(Hz)	w_2(Hz)	w_3(Hz)
0	-	1.486	4.372	7.003
1	k_2=0.9k_2	1.464	4.356	6.996
2	k_2=0.8k_2	1.438	4.337	6.987
3	k_2=0.5k_2	1.317	4.252	6.832
4	k_2=0.8k_2,k_4=0.8k_4	1.416	4.223	6.933

For statistical computation, the simulated data series is divided into 2000 segments. Under baseline condition, the first 1000 segments are used as training set to obtain mean and variance of MD, and the latter 1000 segments are used to calculate MD indices as validation reference. For damaged cases, only the last 1000 segments are used to evaluate MD indexes, ending up with the same number of MD indices as baseline case for statistical comparison.

4.2 Experimental structure

The laboratory experiment from the ASCE benchmark structure [31], which is a 4-story, 2-bay by 2-bay steel-frame scale-model structure, is shown in Fig. 3 and is subsequently used to test the proposed method on a much more realistic testbed. Details about this experiment can be found in the website at http://www.ca.cityu.edu.hk/asce.shm/. The nominal structure with all braces in place is denoted as baseline condition, and damage is simulated by removing various braces in the structure. Damage cases are listed in Table 2.

Table 2: Damage sceneries of the experiment structure

case	Damage description
1	Removed braces on 1st floor in one bay on southeast corner
2	Removed braces on 1st and 4th floors in one bay on southeast corner
3	Removed braces on all floors in one bay on southeast corner
4	Removed all braces on east side

Stochastic excitation was applied by a shaker on top of the structure, and acceleration responses were measured by gauges placed near the center column of the frame at each floor, DasyLab Acquisition system is used to acquire data and the sampling frequency is 250 Hz [32].

Figure 3: Diagram of the ASCE benchmark structure under case 2[31]

5 Test description

5.1 Computational model results

5.1.1 Attractor reconstruction parameters

For optimal time delay selection, since the same result will be acquired by using any segment data under healthy and damaged condition, only typical result from one segment is shown in Fig. 4(a) for the sake of brevity. As the first minimum of AMI will be reached at time delay T= 2 for all sensor channels; hence the delay T is set to 2 for global embedding. Fig.4 (b) shows the FNN function of a random selected segment. It shows that the percentage of FNN function declines rapidly and firstly approaches zero at M=5 for sensor channel 1 and 2, while M=6 for others sensor channels. The shape of the FNN function imitates the functions from a known deterministic signal (for example, Lorenz signal) very well, since they both contain most of their information in the first few dimensions.

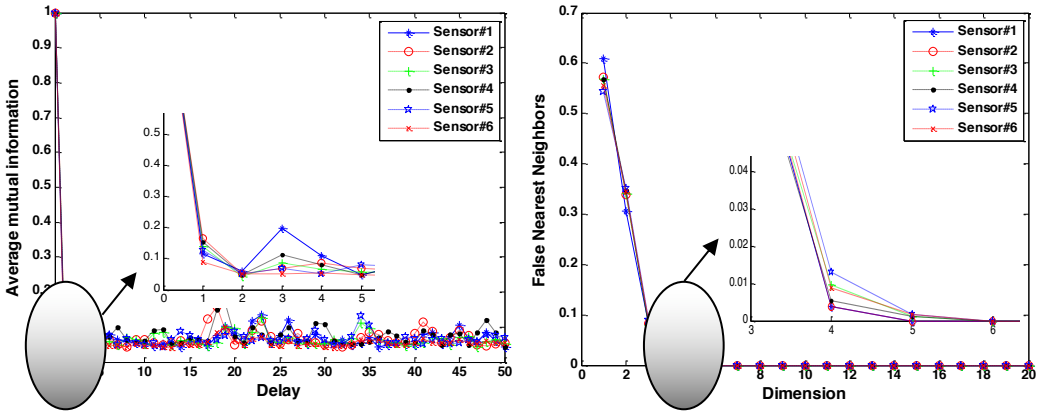

(a) (b)

Figure 4: Optimal embedding parameter selection for simulated data (a) AMI (b) FNN

In order to investigate the proper embedding dimension for all segments, the average optimal dimensions of all segments under baseline condition for all sensors from FNN function are listed in Table 3.

Table 3: Average proper embedding dimension under baseline condition

Sensor number	1	2	3	4	5	6
Optimal dimension	5	5	5	5	6	6

5.1.2 Damage detection performance

The distributions of the MD index under baseline and damaged condition are both tested using Kolmogorov-Smirnov goodness-of-fit hypothesis, and the normal distribution is not rejected under significance level 0.05. Therefore, normal distributions of MD from damage case 1 to 4 for the numerical simulation study are plotted in Figure 5.

It is observed that there is a clear separation of MD distribution between baseline and damage cases from 2 to 4. The ROC curve is near random guess line under damage case 1 (AUC=0.7152), indicating that damage detection ability is fair under this situation. However, the detection performance will increase significantly as damage grows: for example, the AUC increases to 0.8785 under case 2, indicating that the damage can be identified successfully by the proposed method. Moreover, Fig. 5(a) shows that the variance of MD distribution will decline when damage occurs from one place to two places.

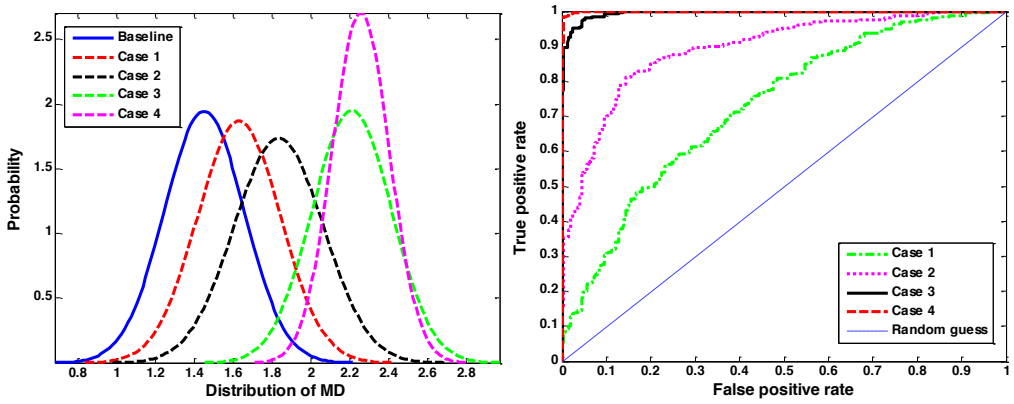

(a) (b)

Figure 5: Damage detection (a) Distribution of MD (b) ROC curve

If no embedding strategy is adopted, the distributions of MD under different damage cases and the corresponding ROC curves are plotted in Fig.6., and then the comparison of AUCs is presented in Table 4. For damage cases 3 and 4, the detection is decisive; however, for less severe conditions, discrimination of the damaged case from baseline is harder, although early warning is critically important for maintenance schedule. This phenomenon indicates that damage is almost impossibly discerned just using SVD method.

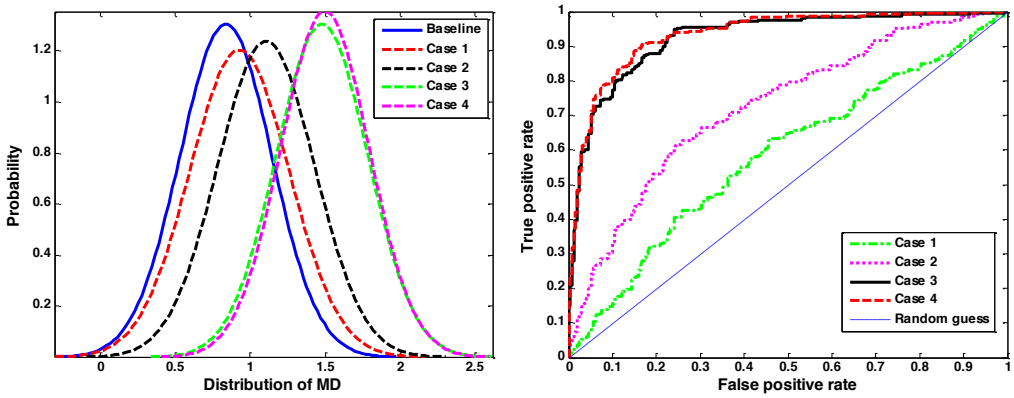

(a) (b)

Figure 6: Damage detection without embedding (a) Distribution of MD (b) ROC curve

Table 4 shows that the AUCs with embedding will increase under all damage cases in contrast to values without embedding, and this indicates that damage detection ability will be improved by the proposed method.

Table 4: Area under ROC curve without and with embedding

Damage Case	1	2	3	4

AUCs (without embedding)	0.5801	0.7184	0.9212	0.9311
AUCs (with embedding)	0.7151	0.8785	0.9925	0.9986
Relative increment percent (%)	23.30	22.28	7.84	7.25

5.1.3 Damage severity identification

Fig. 7 shows the DC index under different damage levels. It is evidently observed that DCs increase almost linearly with damage progression, when embedding strategy is used, meaning that relative damage severity can be easily identified even direct quantification of damage cannot be achieved. However, DCs with embedded state space greatly enhance the sensitivity of detection, and for each damage case, the DC evaluations get doubled compared to the DC without embedding.

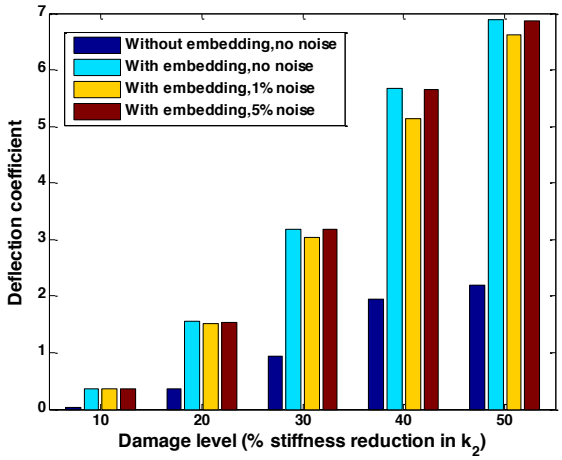

Figure 7: DCs under different damage severity

5.1.4 Damage detection with noise

In order to further investigate the effectiveness of the proposed damage detection method, a more stringent test condition is considered. The distributions of MD under damage case 1 and 3 with different noise levels (artificial contamination) are presented in Fig.8 and the AUCs are listed in Table 5, and DCs are plotted in Fig. 7. It is observed that the mean of MD distribution will increase to a certain extent with noise data both under reference and damaged condition in Fig. 8, the listed AUCs and DCs for different contamination levels show no significant changes compared to the performance of noise-free cases, demonstrating the noise robustness of this proposed method.

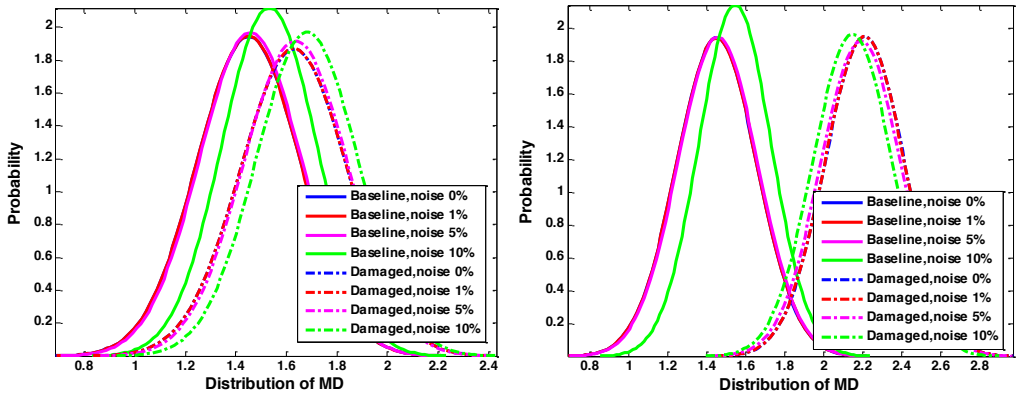

(a) (b)

Figure 8: Distribution of MD with noise: (a) case 1 (b) case 3

Table 5: Area under ROC curve for the benchmark structure

Noise level	0%	1%	5%	10%
Case1	0.7152	0.7183	0.7148	0.7100
Case3	0.9925	0.9928	0.9924	0.9886

Fig. 9 shows the variation trend of average MD with differential noise level. It is observed that the trend between MD and noise level is nonlinear, the average MD increases very slowly when the noise level is under 10 percent both at baseline and damaged conditions, but it will increase very rapidly when the noise level increases. Although the proposed methods cannot detect damage successfully when the magnitude of noise is over 20% of the amplitude of measured data, its performance is still quite good when noise level is below 10%.

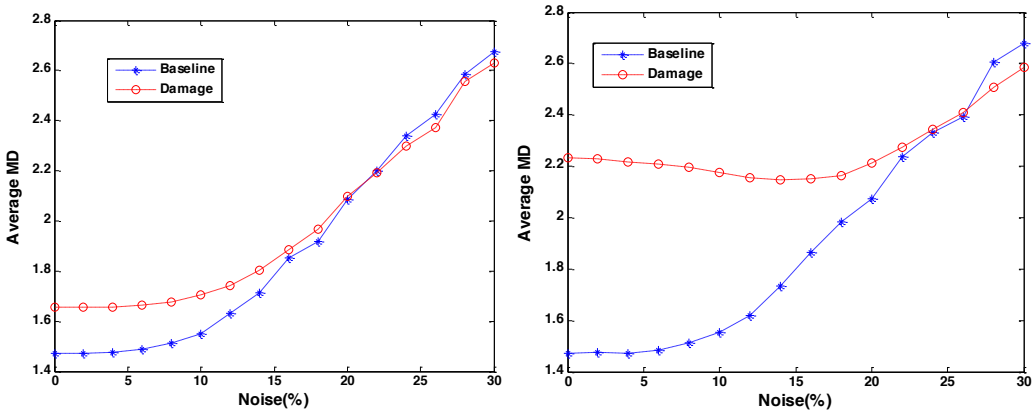

(a) (b)

Figure 9: variation trend of average MD with noise, (a) case1 (b) case 3

5.2 Experimental data results

5.2.1 Attractor reconstruction parameters

The Optimal embedding parameter selection is presented in Fig. 10. Fig. 10 (a) shows that AMI function reaches its first minimum at time delay T=2 for each sensor, and Fig. 10 (b) indicates that FNN functions drop to 0 at dimension 5 for all sensors. Thus the time delay is set to 2 and embedding dimension is set to 5 for all sensors for the benchmark structure data.

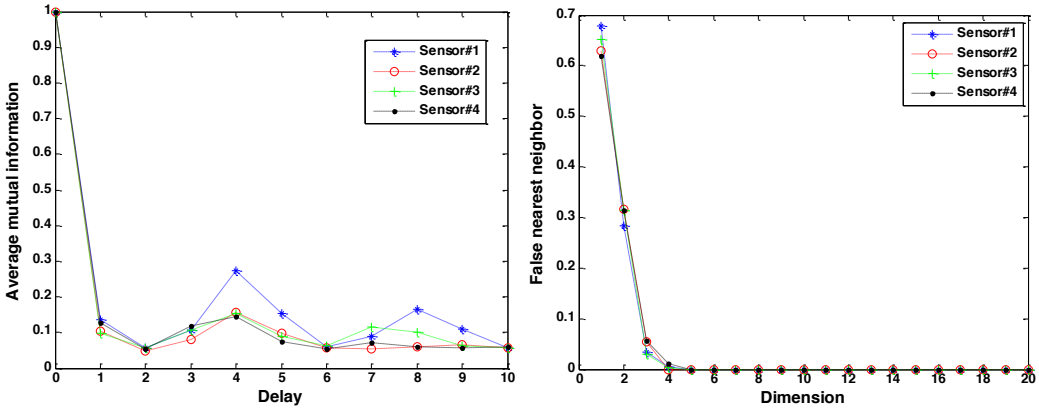

(a) (b)

Figure 10: Optimal embedding parameter selection (a) AMI (b) FNN

5.2.2 Damage detection performance

Since the size of data measured from the experiment is insufficient for statistical analysis, segments used to reconstructed attractor will overlap with adjacent segments with 50% sampling data. The hypothesis that distribution of the MD is normal cannot be rejected under significance level 0.05. In order to compare the proposed method with the traditional approach that excludes embedding, the normal distribution of MD under different damage cases are depicted in Figs. 11 and AUCs are listed in Table 6.

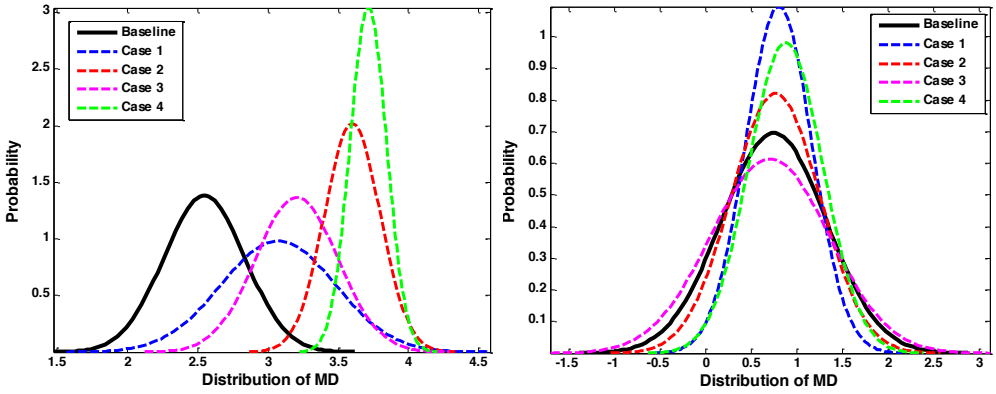

Figure 11: Distribution of MD under different damage cases (a) with embedding (b) without embedding

It is observed that if no embedding strategy is implemented, it is difficult to discern damage in all cases in Figs. 11(b) since the MD distribution overlap with the MD distribution under baseline. While it can successful detect the damage using the proposed method in Figs. 11(a). Moreover, just like the 6 DOF system, the more places in which damage occurs, the less the variance of the MD distribution is in Figs. 11(a). Hence, it can reasonably be inferred that the number of damage locations can be somewhat, although not exactly, estimated. Finally, table 6 shows that the damage detection performance will be improved also with embedding under all damage cases.

Table 6: Area under ROC curve for the benchmark structure

Damage Case	1	2	3	4
AUC(without embedding)	0.4991	0.5124	0.5562	0.5559
AUC(with embedding)	0.8203	0.9943	0.9446	0.9943

5.2.3 Damage severity

Fig. 12 shows DCs under different damage levels. DCs increase when the damage goes severe, since damage deteriorates from case 1 to 4 in which 1, 2, 4 and 8 braces are removed step-by-step. Therefore the approach is successful for identifying the damage severity in the benchmark problem.

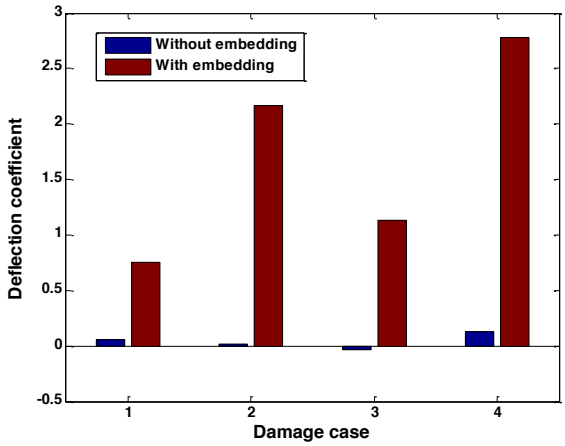

Figure 12: DCs under different damage severity for the benchmark structure

6 Conclusions

Observing that boundary of the reconstructed attractor can vary with different system states, a multivariate damage detection method was presented in this paper. The acceleration time series of all sensor channels under stochastic excitation are embedded globally, and Mahalanobis distance of the singular value vectors acquired from the reconstructed attractors are used as detection feature. Two statistical indexes, AUC and DC, are used as metrics based on Mahalanobis distance to identify the presence and severity of damage. Since most state-space-based method can only detect damage successfully under deterministic excitations (such as a chaotic input), and this is impractical for civil infrastructure applications, the proposed method shows the capability of state-space-based damage detection via stochastic excitations. The proposed method is also computationally efficient, since seeking neighbor points is no longer needed, as required by the conventional state-phase-based methods using attractor predictive error features.

Performance of the proposed method is demonstrated by numerical simulation study of a 6 degree-of-freedom system and the IASC-ASCE 4-story benchmark experimental structure. Results obtained from the 6 degree-of-freedom system demonstrate that the damage can be identified satisfactorily by AUC index. Although direct quantification of damage cannot be achieved, the increase of DCs can be used to estimate the relative severity of the damages. Furthermore, performance of damage detection capability using the proposed methodology will not degrade even when extraneous noise level is as high as 10%. The same conclusion from the benchmark structure can be made that the presence and severity of the damage are identified successfully.

The proposed method shows reasonable promise, and further study will be focused upon embedding parameter selection and in-situ factors influence, including operational and environmental uncertainties.

Acknowledgement

The authors would like to thank ASCE benchmark group for the experiment data and the first and fourth author would like to thank the support from the fundamental research funds for the central universities in China (CDJRC10200018, CDJZR11200010, and CDJZR12200060) and from Chongqing Science & Technology commission (cstc2012jjA30006). The second and third author would like to acknowledge the Air Force Office of Scientific Research (AFOSR) Grant #FA9550-10-1-0455 (Dr. David Stargel, Program Manager) for support of part of this work.

References:

1. Doebling SW, Farrar CR and Prime MB. A summary review of vibration-based damage identification methods. *Shock Vib Dig* 1998; 30:91-105.
2. Sohn H, Farrar CR, Hemez FM, et al. A Review of Structural Health Monitoring Literature: 1996-2001. LA-13976-MS, February, 2004. Los Alamos, NM: Los Alamos National Laboratory.
3. Farrar CF and Worden K. An introduction to structural health monitoring. Philos. *Trans. R. Soc. A* 2007; 365:303-315.
4. Friswell MI. Damage identification using inverse methods. *Philos. Trans. R. Soc A* 2007; 365:393-410.
5. Farrar CR and Jauregui DA. Comparative study of damage identification algorithms applied to a bridge: II numerical study, *Smart Mater Struct* 1998; 7:720-731.
6. Yao Ruigen, Shamim N and Pakzad. Autoregressive statistical pattern recognition algorithms for damage detection in civil structures. *Mech Syst Signal PR* 2012; 31:355-368.
7. Nair KK, Kiremidjian AS and Law KH. Time series-based damage detection and localization algorithm with application to the ASCE benchmark structure. *J Sound Vib* 2006; 291:349-368.
8. Tomoo Saito1 and Beck JL. Bayesian model selection for ARX models and its application to structural health monitoring. *Earthquake Eng Struc* 2010; 39: 1737-1759.
9. Gul M and Catbas F. Damage Assessment with Ambient Vibration Data Using a Novel Time Series Analysis Methodology. *J Struct Eng(ASCE)* 2011; 137:1518-1526.
10. N. Wu and Q. Wang. Experimental studies on damage detection of beam structures with wavelet transform. *Int J Eng Sci* 2011; 49:253-261.
11. Roveri N and Carcaterra A. Damage detection in structures under traveling loads by Hilbert-Huang transform. *Mech Syst Signal PR* 2012; 28:128-144.
12. Todd MD, Nichols JM, Pecora LM, et al. Vibration-based damage assessment utilizing state space geometry changes: local attractor variance ratio. *Smart Mater Struct* 2001; 10:1000-1008.
13. Nichols JM, Todd MD, Seaver M, et al. Use of chaotic excitation and attractor property analysis in structural health monitoring. *Phys Rev E* 2003; 67:0162091-0162098.
14. Nichols JM, Nichols CJ, Todd MD, et al. Use of data driven phase space models in assessing the strength of a bolted connection in a composite beam, *Smart Mater Struct* 2004;132:41-50.
15. Overbey LA and Todd MD. Damage Assessment using Generalized State-Space Correlation Features. *Struct Health Monit* 2008; 7:347-363.
16. Trendafoilova I, Gorman DG and Manoach E. An Investigation on Vibration-based Damage Detection in Circular Plates. *Struct Health Monit* 2009; 8:291-302.

17. Moniza L, Nichols JM and Nichols CJ. A multivariate, attractor-based approach to structural health monitoring. *J Sound Vib* 2005; 283:295-310.

18. Torkamani S, Eric A, Butcher, et al. Hyperchaotic probe for damage identification using nonlinear prediction error. *Mech Syst Signal PR* 2012; 29:457-473.

19. Nichols JM. Structural health monitoring of offshore structures using ambient excitation. *Appl Ocean Res* 2003; 25:101-114.

20. Overbey LA, Olson CC and Todd MD. A parametric investigation of state-space-based prediction error methods with stochastic excitation for structural health monitoring, *Smart Mater Struct*, 2007; 16:1621-1638.

21. Nie Zhenhua, Hao Hong and Ma Hongwei. Using vibration phase space topology changes for structural damage detection, *Struct Health Monit* 2012;5:538-557.

22. Pecora LM, Moniz L, Nichols J, et al. A unified approach to attractor reconstruction, *Chaos* 2007; 17: 013110-013119.

23. Figueiredo E and Todd MD. Autoregressive modeling with state-space embedding vectors for damage detection under operational variability. *Int J Eng Sci* 2010; 48:822-834.

24. Knapp C and Carter G.The generalized correlation method for estimation of time delay. *IEEE T Acoust Speech* 1976; 24:320-327

25. Fraser AM and Swinney HL. Independent coordinates for strange attractors from mutual information. *Phys Rev A* 1986; 33:1134-1140.

26. Broomhead DS and King GP. Extracting qualitative dynamics from experimental data. *Phys Rev D* 1986; 20:217-236.

27. Kennel MB, Brown Reggie, Abarbanel HI. Determining embedding dimension for phase-space reconstruction using a geometrical construction. *Phys Rev A* 1992; 45:3403-3411.

28. Zang C, Friswell MI and Imregun M. Structural Damage Detection using Independent Component Analysis. *Struct Health Monit* 2004; 3:69-83.

29. Markou M and Singh S. Novelty detection: a review-part 1: statistical approaches. *Signal Process* 2003; 83:2481-2497.

30. Søreide K. Receiver-operating characteristic curve analysis in diagnostic, prognostic and predictive biomarker research. *J Clin Pathol* 2009; 62:1-5

31. Dyke SJ, Bernal D, Beck J, et al. Experimental phase 2 of the structural health monitoring benchmark problem. In 16th ASCE Engineering Mechanics Conference, Seattle, Washington,ASCE, 16-18 July, 2003.

32. IASC-ASCE Structural Health Monitoring Task Group Web Page: http://wusceel. cive. wustl. edu/asce.shm/